Journal of
Composites Science

Article

Effect of Photo-Crosslinking Conditions on Thermal Conductivity of Photo-Curable Ladder-like Polysilsesquioxane–Al_2O_3 Nanocomposites

Chiara Romeo [1,*], Giulia Fredi [1], Emanuela Callone [2], Francesco Parrino [1] and Sandra Dirè [1,2,*]

[1] Department of Industrial Engineering, University of Trento, Via Sommarive 9, 38123 Trento, Italy; giulia.fredi@unitn.it (G.F.); francesco.parrino@unitn.it (F.P.)
[2] "Klaus Müller" Magnetic Resonance Lab., Department of Industrial Engineering, University of Trento, Via Sommarive 9, 38123 Trento, Italy; emanuela.callone@unitn.it
* Correspondence: chiara.romeo@unitn.it (C.R.); sandra.dire@unitn.it (S.D.)

Abstract: The miniaturization and high-power density of modern electronic devices pose significant thermal management issues, particularly affecting their performance and lifetime. Ladder-like polysilsesquioxanes (LPSQs) offer a promising solution due to their remarkable thermal, mechanical, and chemical properties. By incorporating thermally conductive fillers, LPSQ composites can achieve high thermal conductivity (TC), making them ideal for thermal management in advanced electronic applications. In this study, LPSQ-based nanocomposites containing functionalized alumina nanoparticles were prepared by solution casting and UV curing, and the effects of varying amounts of Irgacure-184 photoinitiator on their structural and thermal properties were investigated. Three sets of samples were prepared with a fixed amount of LPSQs, 80 wt.% of nanoparticles, and 1, 5, or 10 wt.% of photoinitiator with respect to the matrix. TC was evaluated from the measured values of heat capacity, density, and thermal diffusivity. TC values increased by 60%, 71.2%, and 93.1% for the three samples, respectively, compared to the neat matrix. Results indicate that an intermediate amount of photoinitiator (5%) preserved LPSQs' structural integrity, namely the presence of long linear silsesquioxane chains, and provided good filler dispersion and distribution, high polymerization degree, thermal stability, and high TC.

Keywords: thermal conductivity; ladder-like polysilsesquioxanes; photoinitiator; crosslinking degree; filler dispersion; solid state nuclear magnetic resonance; nanocomposites

check for updates

Citation: Romeo, C.; Fredi, G.; Callone, E.; Parrino, F.; Dirè, S. Effect of Photo-Crosslinking Conditions on Thermal Conductivity of Photo-Curable Ladder-like Polysilsesquioxane–Al_2O_3 Nanocomposites. *J. Compos. Sci.* **2024**, *8*, 295. https://doi.org/10.3390/jcs8080295

Academic Editor: Chi-Hui Tsou

Received: 11 June 2024
Revised: 11 July 2024
Accepted: 25 July 2024
Published: 1 August 2024

1. Introduction

Effective thermal management is a crucial challenge in various technological and industrial applications, ranging from microelectronics to automotive and aerospace engineering. The continual miniaturization and increasing power density of advanced electronics require suitable materials capable of efficient heat dissipation. Inadequate thermal management can lead to overheating issues, which may compromise the performance, reliability, and lifetime of electronic devices.

In this regard, thermal management materials are designed to address these challenges by enhancing heat transfer and dissipation. The aim is to offer remarkable properties tailored to specific applications, primarily high thermal conductivity (TC), in addition to good mechanical compliance and stability under operating conditions. Therefore, the development of novel thermal management materials, such as carbon-based materials [1], metal matrix composites [2], and polymer composites [3], is the focus of research in materials science. These innovations leverage the exceptional thermal properties of constituent materials, providing pathways for enhanced thermal performance. Graphene and carbon nanotubes exhibit extraordinary thermal conductivity, making them ideal candidates for next-generation thermal interface materials [4,5]. However, in the field of electronics, materials for electronic packaging must also possess electrical insulation, good processing ability, flexibility, and corrosion resistance. In this frame, polymer composites with enhanced TC gained significant interest and have proven to be effective substitutes for traditionally used materials in heat dissipation applications within the electronics industry [6]. Composites filled with carbon, metal, or ceramic particles show significantly higher thermal conductivity with respect to the neat matrices. Thermal conductivity increases with filler content and decreases with the decreasing size of particles and aggregates; moreover, polydispersed fillers, i.e., a mixture of different-sized particles, appear more effective than monodispersed ones [7]. For instance, Shikun et al. investigated the thermal conductivity and heat flux distributions of alumina (Al_2O_3)-filled composites, showing that high thermal conductivity can be achieved by multiscale fillers and by regulating their size-matching effect [8]. However, the most relevant issues are related to composite processing, which is crucial in reducing thermal transport resistance. Achieving homogenous filler dispersion and continuous conductive paths, as well as limiting interfacial flaws and increasing filler-matrix compatibility, are some of the main goals [6,7]. Therefore, tuning the properties of matrix and filler and properly selecting processing parameters can effectively enhance thermal conductivity in polymer heat exchangers.

A promising alternative, only recently explored, is given by the organosilicon compounds known as polysilsesquioxanes (PSQs), with chemical formula $[RSiO_{1.5}]_n$, in which every silicon atom shares three bridging oxygen atoms, and R is a hydrogen atom or an organic functional group [9]. PSQs are mainly synthesized through hydrolysis–condensation reactions of trialkoxysilanes; by tailoring the synthesis parameters and depending on the nature of the R group, they can be obtained in different architectures, from polyhedral oligomeric silsesquioxanes (POSSs) to random-structured and ladder-type polysilsesquioxanes (LPSQs) [10,11]. Due to their limited solubility and difficulties in achieving a homogeneous composite, POSSs are primarily used as additive or crosslinkers. In contrast, LPSQs overcome these limitations, enabling their application in free-standing films [12], making them ideal candidates for electronics, coatings, and high-performance composites [13–18].

LPSQs are characterized by a linear, double-stranded siloxane backbone, forming a regular and extended two-dimensional network. This structure ensures high thermal stability [19] and excellent mechanical properties, including high tensile strength and elasticity [20]. LPSQs typically exhibit low coefficients of thermal expansion, reducing the risk of thermal stress and mechanical failure in electronic components [20]. Moreover, LPSQs can be easily integrated with other materials and systems, making them versatile for various composite and hybrid material designs. This compatibility is essential in proposing advanced thermal management solutions that combine multiple materials to achieve the desired balance of properties.

Although polysilsesquioxanes generally have moderate thermal conductivity, by incorporating fillers such as graphene, carbon nanotubes, and metallic or ceramic nanoparticles into the PSQs matrix, it is possible to significantly improve their heat dissipation capabilities. Among the different types of high-TC filler nanoparticles, ceramic fillers have lower TC (e.g., 30–300 W/m K [6]), but they can provide electrical insulation, making them suitable in the preparation of nanocomposites (NCs) for electronic applications. Polymer composites with ceramic fillers exhibit high thermal stability, high-temperature endurance, and reduced shrinkage effects compared to metal-containing ones [7]. Alumina is a promising filler due to its relatively high thermal conductivity (25–40 W/m K), low cost (1–10 $/kg), non-toxic nature, high physical and chemical stability, versatile synthesis, and high electrical resistivity (>10^{14} Ω cm). Alumina fillers have been incorporated into various polymers, such as polyurethane [21], silicone rubber [22], polybutadiene [23], polyvinyl alcohol [24], and bacterial cellulose [25], to create functional composites with enhanced TC.

For instance, Liu et al. used alumina as a filler to obtain thermally conductive silicone rubbers (TCSRs). With a filler loading level of 96 wt%, the TCSR reached a high and isotropic thermal conductivity of 8.4 W/m K and a high dielectric strength (>6 kV/mm) [22].

Ouyang et al. fabricated a network of Al_2O_3 spheres and used them as fillers for a phenolic resin (PR), achieving a thermal conductivity of 4.01 W/m K, enhanced by 1800% compared with the neat matrix. [26]. In our previous work [27], we showed the large potential of ladder-like poly(methacryloxypropyl) silsesquioxanes (LPMASQs) for the development of high thermally conductive nanocomposites. LPMASQs were employed both alone and blended with *cis*-polybutadiene as matrices for dispersing alumina nanoparticles. Moreover, the research highlighted the remarkable effect of nanoparticles' surface functionalization on the filler dispersion and the thermal conductivity of the final composites. The importance of particles' functionalization was also observed by Ahn, as Al_2O_3 functionalized nanoparticles were readily incorporated into the polymer matrix via multiple linkages with the LPSQs [28].

Given this background and based upon the findings of the previous work of Mingarelli et al. [27], this article aims to deepen the factors that can influence the thermal conductivity of photocurable ladder-like polysilsesquioxane–Al_2O_3 nanocomposites. Thermal conductivity is highly dependent on the configuration and conformation of the polymeric chains [3]. Additionally, crosslinks can establish efficient heat conduction pathways by connecting polymer chains through strong covalent bonds [29,30]. Therefore, it appears crucial to improve the reactivity towards polymerization of the functional organic groups by controlling the polymer architecture at the same time.

The choice between photo-crosslinking and thermal crosslinking depends on specific application requirements, desired material properties, and processing constraints. Nevertheless, ultraviolet (UV) curing is a faster and more ecological alternative to conventional thermal curing. In UV curing, a free radical polymerization reaction is initiated by UV light rather than heat. Key advantages of UV curing include precise control over initiation timing, rapid curing (from seconds to several minutes), and no temperature requirement, leading to greater productivity and energy efficiency [31–33]. However, limitations include difficulties in curing thick or pigmented systems due to limited light penetration [31] and susceptibility to oxygen inhibition, necessitating an inert environment [34]. A UV curing system requires a monomer and a photoinitiator [35]. Common monofunctional monomers include unsaturated and acrylate monomers [36]. Considering cyclic olefin monomers, chain-growth polymerization occurs via ring-opening metathesis polymerization (ROMP) using heterogeneous and homogeneous catalysts [37]. Żak et al. studied the applications of olefin metathesis in the synthesis of POSS and POSS-based materials [38]. Even if the method offers numerous advantages for their synthesis, it is limited by the small number of monomers susceptible to ROMP. The monomer concentration affects the polymer's rigidity: higher concentrations lead to longer crosslink chains and a more flexible polymer, reducing stiffness and the risk of cracking upon minor impacts [31]. Photo-crosslinking is generally preferred for LPSQs due to its ability to provide precise control, lower processing temperatures, and enhanced material stability [39]. This makes photo-crosslinking particularly advantageous for applications in microelectronics, where precision and material integrity are critical. In light of this, this study focused on investigating the influence of a variable amount of photoinitiator on the structural properties of LPMASQ/alumina composites. This approach aimed to increase the degree of crosslinking, thereby enhancing the overall thermal conductivity while maintaining its linear structure as much as possible. In detail, filler dispersion, degree of crosslinking, matrix structural properties, and thermal conductivity of the nanocomposites were studied. With the ultimate goal of achieving composites with enhanced thermal conductivity, a fairly high amount of particle load was required. In this respect, the LPMASQ matrix was loaded with 80 wt.% of Al_2O_3 nanoparticles functionalized with methacryloxypropyl trimethoxysilane (MPTMS), adding different amounts of Irgacure-184 photoinitiator. Nanocomposite films were prepared by a simple solvent-casting technique followed by UV curing. NC structural properties were characterized by Fourier transform infrared spectroscopy (FTIR), solid-state nuclear magnetic resonance (SS-NMR), scanning electron microscopy (SEM), and thermogravimetric analysis (TGA), while TC was evaluated from the values of sample density, specific heat capacity, and thermal diffusivity.

2. Materials and Methods

2.1. Materials

Gamma alumina nanoparticles (99.5%, NanoArcTM, AL-0405, average particles diameter 48 nm, specific surface area SSA 34 m^2/g) were obtained from Alfa Aesar (Haverhill, MA, USA). 3-Methacryloxypropyl trimethoxysilane (98%, MPTMS) was obtained from ABCR GmbH (Karlsruhe, Germany). Ethanol absolute anhydrous (EtOH $\geq$ 99.9%) was purchased from Carlo Erba reagents (Milan, Italy). Toluene (99.8%), tetrahydrofuran (99.9%, THF), potassium carbonate ($K_2CO_3 \geq 99.0\%$), and 1-hydroxycyclohexyl phenyl ketone (99%, Irgacure 184, I-184) were purchased from Sigma-Aldrich (St. Louis, MO, USA).

2.2. Sample Preparation

Synthesis of LPMASQ. The MPTMS-capped ladder-like silsesquioxane was prepared by the sol–gel process from methacryloxypropyl trimethoxysilane. A schematic representation of the established procedure [27,40–42] is detailed in the Supplementary Information (Scheme S1). Briefly, MPTMS (0.08 mol) was added dropwise in a mixture of H_2O (0.27 mol) and THF (0.11 mol) in the presence of K_2CO_3 as catalyst (0.0003 mol) under nitrogen flow. The pale-white solution was vigorously stirred at room temperature, in the dark, in N_2 atmosphere, for 10 days. Afterward, a transparent glue-like product was obtained through solvent evaporation at 30 °C under mild vacuum. The obtained product was stored in the dark in a desiccator under N_2 atmosphere.

Synthesis of MPTMS-capped alumina NPs. MPTMS-capped Al_2O_3 nanoparticles, labeled as MPTMS@Al_2O_3, were synthesized according to our previous report [27]. In detail, 2 g of commercial nano γ-Al_2O_3 were dispersed by sonication (15 min) in toluene (50 mL) and then put under reflux conditions. MPTMS (830 μL) was added dropwise, and the suspension was kept under reflux at 120 °C and vigorous stirring for 24 h (Scheme S2). The obtained nanoparticles were purified by centrifugation at 4500 rpm for 15 min and washed twice with toluene and once with ethanol. Finally, they were dried overnight in a vacuum oven at 80 °C.

Preparation of LPMASQ/MPTMS@Al_2O_3 nanocomposites. LPMASQ nanocomposites were prepared, as reported in our previous work [27], through a slightly modified solvent casting technique (Scheme S3). Three samples were prepared (Table 1); they were synthesized following the same procedure but varying the amount of photoinitiator, which was, respectively, 1, 5, and 10 wt.% with respect to the LPMASQ matrix. LPMASQ (1 g) was dissolved at RT in THF (1 mL). A total of 0.8 g of MPTMS@Al_2O_3 was suspended by sonication (15 min) in 2 mL of THF and then added under stirring into the ladder solution. In total, 10, 50, and 100 mg of Irgacure-184 photoinitiator were dissolved in THF (0.5 mL) and added to the three sample solutions, respectively. The mixtures were kept stirring in the dark for 30 min and then drop-casted into polypropylene (PP) Petri dishes. Solvent evaporation was performed in a vacuum oven at 30 °C under mild vacuum for 2 h, avoiding exposure to light. The dried composites were photo-crosslinked under N_2 flow into a cooled isolated chamber using a mercury vapor lamp (HBO 50 W/AC 39 V, OSRAM, curing time 15 min, specimen–lamp distance 13 cm). During this process, the samples were kept at a temperature range of 0–6 °C using an ice bath. The dried composites were irradiated for 10 min on the top side and then 5 min on the bottom side to improve sample photo-crosslinking. The obtained nanocomposites were stored in a desiccator, in the dark, and in a nitrogen atmosphere. The samples were labeled as 80AF_L (X%), where 80AF stands for 80 wt.% of MPTMS@Al_2O_3 with respect to the LPMASQ (corresponding to 27.5 vol%), L indicates the LPMASQ matrix, and (X%) represents the different amounts of photoinitiator used, namely 1, 5, and 10 wt.% with respect to LPMASQ.

Table 1. Composition of the samples prepared.

Sample	LPMASQ	NPs	I-184
80AF_L (1%)	1 g	0.8 g	0.01 g
80AF_L (5%)	1 g	0.8 g	0.05 g
80AF_L (10%)	1 g	0.8 g	0.1 g

Selected samples were prepared in triplicate and characterized by the techniques reported in the following section.

2.3. Characterization Techniques

FTIR analysis of bare and functionalized alumina nanoparticles was performed in transmittance mode, in the 4000–400 cm^{-1} wavenumber range (64 scans, resolution 4 cm^{-1}), on KBr pellets using a Nicolet Avatar 330 spectrometer (Thermo Fisher Scientific, Waltham, MA, USA). Pristine LPMASQ and nanocomposites were structurally characterized through attenuated total reflectance (ATR) FTIR spectroscopy. ATR-FTIR spectra were acquired in the 4000–550 cm^{-1} wavenumber range (64 scans, resolution 4 cm^{-1}) using a Varian (Palo Alto, CA, USA) 4100 Excalibur spectrometer equipped with a diamond ATR crystal.

^{29}Si, ^{13}C, and ^{1}H NMR spectra of LPMASQ were collected using a Bruker Avance 400WB spectrometer equipped with a BBO 5 mm probe with the following conditions: ^{29}Si: 2k scans, recycle delay 30 s, 79.48 MHz, $\pi/6$ 3.9 μs, and DEPT pulse sequence with 5k scans, recycle delay 4 s, $\pi/2$ 8.8 μs; ^{13}C: 2 k scans, recycle delay 9 s, 100.56 MHz, $\pi/4$ 7.2 μs, power-gated pulse sequence; ^{1}H: 16 scans, recycle delay 5 s, 400.13 MHz, $\pi/4$ 4.8 μs. The sample was diluted in $CDCl_3$ in a 5 mm glass tube. All experiments were conducted at room temperature.

SS-NMR analyses were carried out on MPTMS@Al_2O_3 particles, photo-crosslinked LPMASQ matrix, and LPMASQ nanocomposites using a Bruker 400WB spectrometer operating at a proton frequency of 400.13 MHz. Samples were packed in zirconia rotors (4 mm), which were spun under airflow at 8 kHz. Adamantane and Q_8M_8 were used as external secondary references. NMR experiments were conducted with single pulse and cross-polarization (CP) pulse sequences under the following conditions: ^{13}C frequency: 100.48 MHz, contact time 2 ms, decoupling length 5.9 μs, recycle delay: 5 s, 2 k scans. ^{29}Si frequency: 79.48 MHz, contact time 5 ms, decoupling length 6.3 μs, recycle delay: 10 s, 2 k scans. Single pulse sequence: $\pi/4$ pulse 3.9 μs, recycle delay 300 s, 1 k scans. Profile fitting analyses of NMR spectra were performed with Bruker TopSpin software (version 3.6.4). The results were deemed acceptable, with a confidence level exceeding 95% and a standard deviation of up to ±4%.

To quantify the degree of particles' functionalization, TGA curves of pristine and functionalized alumina nanoparticles were acquired under constant N_2 flow (10.0 mL/min) from 30 °C to 850 °C at a heating rate of 10 °C/min. A Q5000 TA Instruments thermogravimetric analyzer was used. Thermal stability of the photo-crosslinked nanocomposites was studied through TGA analyses, acquired with a Mettler Toledo TG50, in constant airflow (15 mL/min) from 30 °C to 900 °C at a heating rate of 10 °C/min.

Morphological characterization and size distribution of the MPTMS@Al_2O_3 in the nanocomposites were studied with a Carl Zeiss Gemini Supra 40 field emission SEM using secondary electrons as the main source and operating at 7.50 keV. To analyze the fracture surface and minimize crack formation, the composite films were immersed in liquid nitrogen prior to fracturing. A thin metallic coating (Pt/Pd = 80/20) was sputtered on the samples prior to SEM analysis. The size distribution of particles' aggregates was obtained by exploiting Image J software (version 1.53t) from high magnification (80 kX) SEM images, with a standard deviation of up to ±20 nm.

Density values (ρ) of the Al_2O_3 powders, matrix, and LPMASQ/MPTMS@Al_2O_3 nanocomposites were measured at 25 °C using a Micromeritics Multivolume Helium

Pycnometer AccuPyc 1330. ρ values are the result of three independent measurements with a standard deviation of up to ±0.02 g/cm^3.

Specific heat capacity (c_P) of crosslinked LPMASQ of bare and functionalized alumina was evaluated using a Mettler Toledo 30 DSC, according to ASTM E1269 standard, at 25 °C. Specimens were weighed and sealed in aluminum crucibles, then tested at 10 °C/min, from −10 °C to 40 °C, under a nitrogen flow of 50 mL/min. As-obtained specific heat values were used to extrapolate the specific heat of LPMASQ/MPTMS@Al_2O_3 nanocomposites using the mixture rule, as reported in our previous work [27]. c_P values are the result of three independent measurements with a standard deviation of up to ±0.02 J/g K.

Thermal diffusivity (α) of nanocomposites was measured on round-shaped thin films using a Netzsch (Selb, Germany) LFA 467 HyperFlash Light Flash Analyser; measurements were run with a laser voltage of 250 V, pulse width of 30 µs, five pulses per sample, under N_2 flow at 25 °C. Thermal diffusivity of modified and bare Al_2O_3 nanoparticles was analyzed using the same LFA analyzer using a three-layer setup: the powders were pressed between two aluminum discs, applying a clamping torque of 15 cN m, and TC was measured with a laser voltage of 250 V, a pulse width of 600 µs, five pulses per sample, under N_2 flow at 25 °C. Thermal diffusivity was determined using the software Proteus® (NETZSCH, version 8.0.3) provided with the instrument by applying the three-layer model with linear baseline and numerical pulse correction. α values are the result of three independent measurements with a standard deviation of up to ±0.001 mm^2/s.

The thermal conductivity (k) of the composites was calculated from the experimental values of density (ρ, g/cm^3), specific heat capacity (c_P, J/g K), and thermal diffusivity (α, mm^2/s) by the following equation:

$$k = \rho \cdot c_P \cdot \alpha$$

The evaluation of the uncertainty of k was calculated according to the Kline–McClintock model, with a standard deviation of up to ±0.001 W/m K.

3. Results and Discussion

The effect of variable amounts of Irgacure-184 photoinitiator on filler dispersion, degree of crosslinking, matrix structure, and thermal conductivity of LPMASQ/alumina nanocomposites was studied by preparing three samples that differed only in the amount of photoinitiator. The LPMASQ matrix was loaded with 80 wt.% of MPTMS@Al_2O_3 with respect to LPMASQ (equal to a filler volume fraction of 27.5 vol%), adding 1, 5, and 10 wt.% of photoinitiator with respect to LPMASQ. The choice of the amount of particle load was based on the findings of the prior study conducted by Mingarelli et al. [27].

The structural features of synthesized LPMASQ were investigated by FTIR and NMR experiments (Supporting Information, Figure S1). The results were comparable to those from previous studies [27,40]. The presence of a few Si-OH groups (T^2 units) was observed from the FTIR spectrum (Figure S1a), where a very weak band at 3500 cm^{-1} was detected. The strong absorption peaks at 1714 and 1637 cm^{-1} are attributed, respectively, to C=O and C=C stretching vibrations of the methacrylate groups. From the two Si-O antisymmetric stretching vibrations at 1100 and 1020 cm^{-1}, typical of ladder-like structures [12,20], the high intensity of the band at 1020 cm^{-1} indicates a certain degree of structural irregularity. The ^{13}C NMR spectrum (Figure S1b) pointed out both the full hydrolysis of MPTMS methoxy groups and silanol condensation. In agreement with the previous results, the ^{29}Si NMR spectrum (Figure S1c) showed the characteristic LPMASQ backbone given by fully condensed T^3 units (R-Si(OSi)$_3$) centered at about −67 ppm and a small amount of T^2 units (R-Si(OSi)$_2$OH, 2%) at −58 ppm. It is important to maximize condensation since silsesquioxanes that are not highly condensed can act as defects in electronic or coating applications [12]. The presence of several peaks in the T^3 region is due to units in different conformations, as previously reported [40,43].

The effective functionalization of the particles with MPTMS was assessed from FTIR and ^{29}Si and ^{13}C CP MAS NMR spectra (Figure S2). To quantitatively evaluate the functionalization degree, TG analysis was conducted on MPTMS@Al_2O_3 and bare alumina NPs. The net weight loss of functionalized alumina, measured between 150 and 850 °C, was 1.7 wt.%, corresponding to a grafting density of 1.46 molecules/nm^2, which was calculated according to the procedure reported by Zamperlin et al. [44]. Notably, alumina functionalization did not result in significant morphological changes, as previously reported for similar systems [23].

LPMASQ/MPTMS@Al_2O_3 nanocomposites were prepared using a simple solvent-casting technique followed by UV curing in the presence of a variable amount of photoinitiator (Scheme S3). Figure S3 reports the comparison between the spectra of as-synthesized LPMASQ and 80AF_L (1%) nanocomposite. In the nanocomposite, the strong absorption band due to the alumina particles is clearly visible below 900 cm^{-1}, and the intensity of the vinyl band at 1637 cm^{-1} appears reduced with respect to the pristine LPMASQ due to the photoinduced crosslinking of the methacrylate groups.

^{13}C NMR analyses were recorded to quantitatively evaluate the conversion of methacrylate groups as a function of photoinitiator percentage. The ^{13}C NMR spectra of crosslinked composites (Figure 1) showed all the resonances belonging to the LPMASQ matrix. Polymerization was assessed by the decrease of e and g olefinic carbons (138 and 127 ppm, respectively) of the methacrylate group, along with the appearance of two peaks e′ and g′ (57 and 47 ppm, respectively), due to the new methylene carbons created by polymerization of the vinyl group. Additionally, compared to the pristine LPMASQ (Figure S1b), a downfield shifted carbonyl resonance d′ (177 ppm) was also observed, assessing the presence of a carbonyl close to methine e′ and methylene g′. The presence of both d and d′ resonances is then used to quantify the degree of polymerization (DP%) by calculating the ratio between the integration area of d′ and the sum of d and d′ areas (highlighted in Figure 1). For each sample, three distinct batches were prepared and analyzed. The results presented correspond to an average of the measurements made, exhibiting a standard deviation of ±4%.

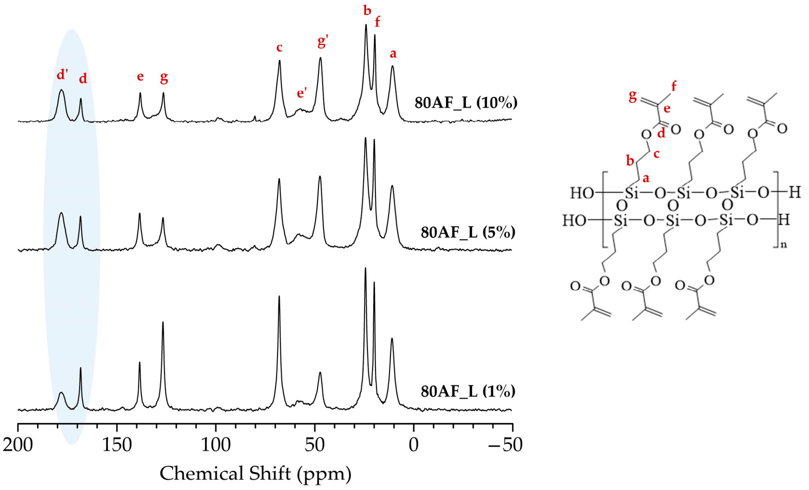

Figure 1. ^{13}C CPMAS NMR spectra of crosslinked nanocomposites; carbon labeling and LPMASQ structure are also shown.

The extent of polymerization increased from 51% to 75% and to 79% with increasing the amount of photoinitiator from 1 to 5 to 10%. It is reasonable to assume that a higher degree of crosslinking promotes the formation of a thermal pathway in the matrix, thereby improving the thermal diffusivity and consequently increasing the thermal conductivity [6,45].

In this regard, the highest amount of photoinitiator warrants a more crosslinked matrix. However, it was observed that the crosslinking process may also lead to a change in ladder conformation [11,40,43]. Notably, to foster the creation of a thermal path conducive to the transmission of phonons, it is required to maximize the presence of elongated, linear chains [6,41]. It is, therefore, essential to analyze the matrix structure subsequent to the photo-curing process. In this respect, ^{29}Si CPMAS NMR experiments were conducted (Figure 2a). Nanocomposite spectra are dominated by the asymmetric resonance centered at about −67 ppm due to T^3 units, which results from the overlapping of the peaks detected in as-synthesized LPMASQ (Figure S1c). Only negligible changes in the T^2/T^3 ratio (Table 2) are found when changing the photoinitiator amount. To evaluate possible structural changes with the variable photoinitiator percentage, lineshape analysis (Figure 2b–d) was conducted following the approach reported by Dirè et al. [40], based on the different linewidth (LW) components that allow to distinguish the conformation of LPMASQ chains. The calculated amounts of each component in the three samples (Table 2) point out that an intermediate quantity of I-184 (5%) enables the maximization of the percentage of linear structures.

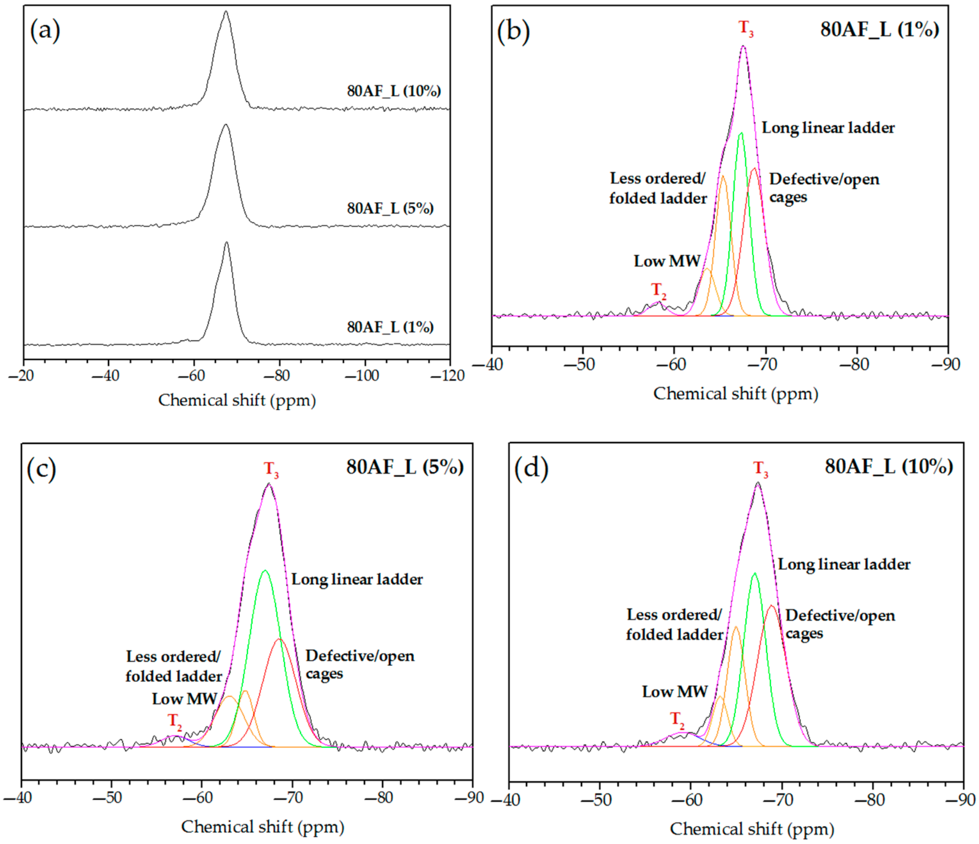

Figure 2. ^{29}Si CPMAS NMR spectra (**a**) of crosslinked nanocomposites and lineshape analyses (**b**–**d**) of the T^3 signal into different linewidth components: low molecular weight, folded ladder, long linear ladder, and defective/open cages.

Table 2. Profile fitting analysis of the ^{29}Si CPMAS spectra (Figure 2b) of the three nanocomposites.

Structures	80AF_L (1%)			80AF_L (5%)			80AF_L (10%)		
	δ (ppm)	LW (Hz)	%	δ (ppm)	LW (Hz)	%	δ (ppm)	LW (Hz)	%
T2	−58.3	168	1.8 (T_2/T_3)	−58.2	268	1.6 (T_2/T_3)	−59.1	282	1.6 (T_2/T_3)
T3_Low MW	−63.5	178	7.3	−63	274	10.7	−63.2	165	6.4
T3_Folded ladder	−65.3	167	23.4	−64.8	174	8.1	−64.9	194	19.1
T3_Long linear ladder	−67.2	175	35.5	−67	344	51.7	−67	258	40.2
T3_Defective/open cages	−68.7	232	33.8	−68.6	384	29.5	−68.8	316	34.3

Morphological characterization was performed on the cross-section surface of the LPMASQ/MPTMS@Al_2O_3 nanocomposites through SEM experiments (Figure 3). Figure 3a–c refer to the fracture surface of the 80AF_L (1%) sample; Figure 3d–f refer to the fracture surface of the 80AF_L (5%) sample; Figure 3g–i refer to the fracture surface of the 80AF_L (10%) sample.

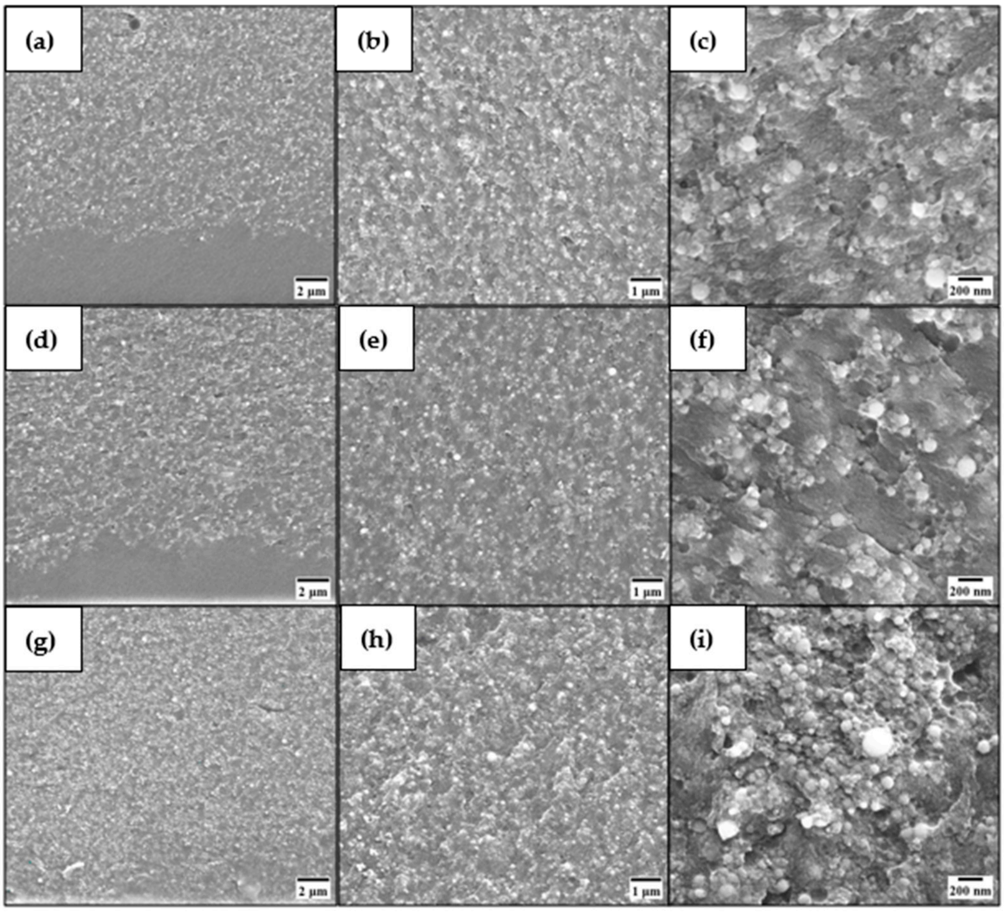

Figure 3. SEM micrographs at different magnification (10kX (**a**,**d**,**g**); 20kX (**b**,**e**,**h**); 80kX (**c**,**f**,**i**)) of 80AF_L (1%) (**a**–**c**), 80AF_L (5%) (**d**–**f**), and 80AF_L (10%) (**g**–**i**) composites. The bottom part of images a, d, and g show the region of particles' depletion present in the upper side of the film.

Low magnification SEM images (Figure 3a,b,d,e,g,h) reveal a homogeneous filler dispersion across all samples. However, upon closer examination of the upper side of the composites (Figure 3a,d,g), it was observed that the lowest concentration of photoinitiator resulted in a 5 µm particle depletion layer. As the amount of photoinitiator increases, this effect decreases, as evidenced in Figure 3d, where a layer of 2–3 µm without particles was observed until it completely disappears, as seen in the fracture surface of the 80AF_L (10%) sample (Figure 3g).

As previously observed [27], the functionalized particles appear embedded in the matrix (Figure 3c,f,i), with small differences among the samples. Therefore, a quantitative analysis of the aggregate size distribution was conducted by exploiting Image J software. The histograms in Figure 4 show a particle size distribution similar to the case of composites with 5 and 10 wt.% of I-184 with respect to LPMASQ. The composite with 1 wt.% of photoinitiator showed a slightly higher presence of particles with lower diameter and, therefore, a lower tendency to form larger aggregates.

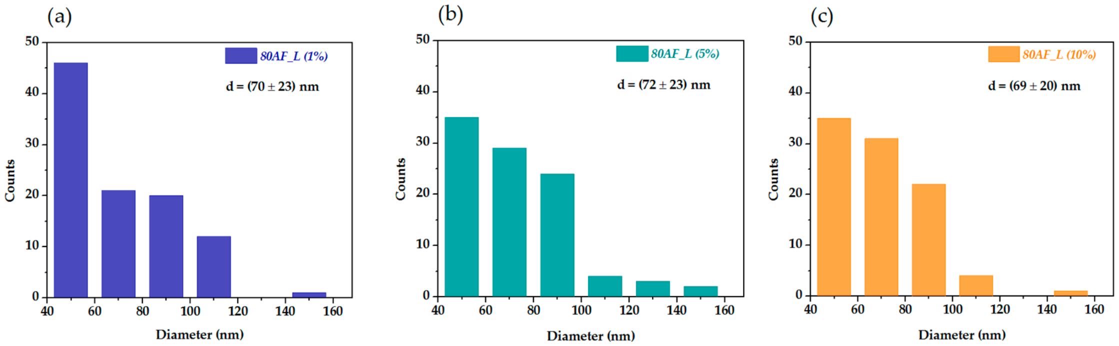

Figure 4. Average size and particle size distribution of 80AF_L (1%) (**a**), 80AF_L (5%) (**b**), and 80AF_L (10%) (**c**). Size distribution of particles' aggregates obtained by Image J software from high magnification SEM images (Figure 3g–i) of the three composites.

The thermal stability of the nanocomposites was evaluated by TG analysis. Thermograms are shown in Figure 5; Table 3 displays the decomposition temperatures T5 and T20, representing the temperatures at which the sample's weight loss reaches 5% and 20%, respectively, along with the residual weight. Thermograms of crosslinked LPMASQ, prepared using 1 wt.% of photoinitiator, are compared with 80AF_L (1%) (Figure 5a). It is noteworthy that the incorporation of the particles improves the thermal stability of the ladder composites. Comparing the three nanocomposites (Figure 5b), an initial observation reveals that the TG curves are similar, each exhibiting an increase in residual mass compared to the crosslinked matrix alone, credited to the inorganic components. However, the sample with 10 wt.% of photoinitiator shows a slight increase in weight loss and appears more unstable than the other two, possibly due to the conformations of the ladder chains formed during the crosslinking process. In detail, the thermal stability of the nanocomposites prepared with 1 and 5 wt.% of I-184 remains almost unchanged; on the contrary, both T5 and T20 of the sample 80AF_L (10%) notably decrease, also with respect to the corresponding temperatures of crosslinked LPMASQ (see values from Table 3).

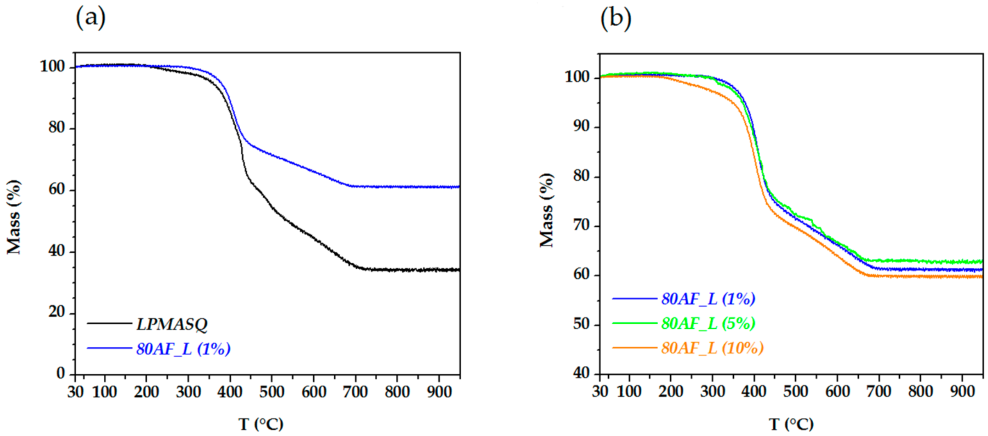

Figure 5. TGA curves of photo-cured LPMASQ and 80AF_L (1%) (**a**) and TGA curve comparison of the three nanocomposites (**b**).

Thermal diffusivity (α) of LPMASQ/alumina nanocomposites was investigated to study the effect of a variable amount of photoinitiator on the establishment of an efficient thermal pathway, potentially resulting in enhanced thermal conductivity (TC) of the composite. TC was calculated as reported in our previous work [27]. Therefore, three parameters were experimentally measured: the density ρ (g/cm^3), the specific heat capacity c_p at constant pressure (J/K g), and the thermal diffusivity α (mm^2/s) at 25 °C. The obtained TC values (k) are reported in Table 4, together with the values of ρ, c_P, and α.

These values were compared with those of the crosslinked LPMASQ, prepared with 1 wt.% of I-184.

Table 3. Results of TG analyses of LPMASQ/alumina nanocomposites: decomposition temperatures T5 and T20, representing the temperatures at which the sample's weight loss reaches 5% and 20%; the residual mass is calculated at 950 °C.

Sample	T5 (°C)	T20 (°C)	Residual Mass (wt.%)
LPMASQ	359	414	34.0
80AF_L (1%)	379	422	61.0
80AF_L (5%)	373	422	62.8
80AF_L (10%)	349	411	59.7

Table 4. Density (ρ), specific heat (c_P), thermal diffusivity (α), and thermal conductivity (k) values of the prepared composite films.

Sample	ρ (g/cm^3)	c_p (J/g K)	α (mm^2/s)	k [W/m K]
LPMASQ	1.23 ± 0.01	1.45 ± 0.01	0.146 ± 0.001	0.260 ± 0.003
80AF_L (1%)	1.69 ± 0.02	1.14 ± 0.02	0.2160 ± 0.0001	0.416 ± 0.008
80AF_L (5%)	1.67 ± 0.01	1.14 ± 0.02	0.2340 ± 0.0005	0.445 ± 0.008
80AF_L (10%)	1.65 ± 0.01	1.14 ± 0.02	0.2670 ± 0.0007	0.502 ± 0.009

The highest amount of I-184, which also promotes the highest degree of polymerization, allows for higher thermal diffusivity values.

Considering the three samples, 80AF_L (1%), 80AF_L (5%), and 80AF_L (10%), thermal conductivity increased by 60%, 71.2%, and 93.1%, respectively, compared to the pristine ladder (photo-cured with 1 wt.% of I-184).

4. Conclusions

In this study, we investigated the effect of variable amounts of Irgacure-184 photoinitiator (1, 5, and 10 wt.% with respect to LPMASQ) on the structural and thermal properties of LPMASQ-based composites containing 80 wt.% of functionalized Al_2O_3 nanoparticles as the filler, with respect to LPMASQ. In fact, the photo-curing conditions play a pivotal role in determining the crosslinking degree and configuration and conformation of the polymeric chains, which eventually affect the overall TC performance.

The study highlights that an intermediate amount of photoinitiator (5%) is a suitable trade-off, providing good thermal stability, thermal conductivity, and structural properties. In particular, increasing the amount of photoinitiator progressively increases the crosslinking degree and reduces the particles' depletion layer that originated during the curing process on the upper side of the NCs. In fact, the sample with the highest amount of photoinitiator (10%) presented no depletion layer and a slightly higher degree of crosslinking (79%) with respect to the sample with 5 wt.% photoinitiator (75%). However, the latter shows the highest percentage of linear silsesquioxane chains, which are necessary to foster the creation of a conductive thermal path, and the highest thermal stability.

Therefore, even if the most relevant TC increase (93.1%) compared to the reference ladder matrix was obtained in the presence of 10 wt.% I-184, an intermediate amount of photoinitiator (i.e., 5 wt.% with respect to LPMASQ) appears to be preferable in the preparation of ladder-like polysilsesquioxane–Al_2O_3 nanocomposites. In fact, it produces a good dispersion of the filler and ensures a high degree of polymerization, thermal conductivity, and thermal stability while keeping the key structural features of the polysilsesquioxane matrix.

The results indicate that LPSQ-Al_2O_3 nanocomposites exhibit significant potential as thermal management materials. They could offer significant advantages in heat dissipation and thermal and chemical stability. Practical applications could include their use as thermal interface materials to improve heat transfer between heat sinks and electronic components (e.g., CPUs, GPUs), in packaging to protect integrated circuits and microprocessors from thermal stress, and as surface coatings to enhance heat dissipation in high-power devices. Additionally, they could improve thermal management in battery systems, power electronics, aerospace and automotive components, and consumer electronics, ensuring better performance and preventing overheating.

Supplementary Materials: The following supporting information can be downloaded at: https://www.mdpi.com/article/10.3390/jcs8080295/s1, Scheme S1: LPMASQ synthesis by controlled base-catalyzed MPTMS hydrolysis–condensation. The reaction yield was 95%; Scheme S2: Synthesis of MPTMS capped alumina nanoparticles. MPTMS was added in a molar ratio of 2:1 with respect to the -OH surface groups of gamma alumina nanoparticles (0.87 mmol/g); Scheme S3: Preparation of LPMASQ/MPTMS@Al_2O_3 nanocomposites; Figure S1: (a) ATR-FTIR spectrum and (b) ^{13}C NMR and (c) ^{29}Si NMR spectra in $CDCl_3$ of as-synthetized LPMASQ; Figure S2: (a) FTIR spectra of neat and functionalized alumina, (b) ^{13}C CPMAS NMR, and (c) ^{29}Si CPMAS NMR spectra of alumina nanoparticles functionalized with MPTMS; Figure S3: FTIR-ATR superimposed spectra of as-synthesized LPMASQ and 80AF_L nanocomposites prepared with 1%wt. Irgacure-184. The inset shows the magnification of the region between 1760 and 1600 cm^{-1} to highlight the reduction in the intensity of the C=C stretching vibration at 1637 cm^{-1} due to crosslinking.

Author Contributions: Conceptualization, S.D. and F.P.; methodology, C.R., G.F., E.C., F.P. and S.D.; validation, C.R., E.C. and G.F.; formal analysis, C.R. and E.C.; investigation, C.R. and E.C.; resources, S.D. and G.F.; data curation, C.R., G.F., E.C. and F.P.; writing—original draft preparation, C.R., S.D. and F.P.; writing—review and editing, C.R., G.F., E.C., F.P. and S.D.; visualization, C.R. and E.C.; supervision, F.P. and S.D.; project administration, S.D., F.P. and G.F.; funding acquisition, S.D., F.P. and G.F. All authors have read and agreed to the published version of the manuscript.

Funding: This work was performed in the frame of the program Departments of Excellence 2023-2027 (DII-UNITN)—Italian Ministry of University and Research (MUR).

Data Availability Statement: The original contributions presented in this study are included in the article/Supplementary Material; further inquiries can be directed to the corresponding authors.

Acknowledgments: Claudia Gavazza and Lorenzo Moschini are acknowledged for their technical support (TGA analysis, SEM observations).

Conflicts of Interest: The authors declare no conflicts of interest.

References

1. Khan, J.; Momin, S.A.; Mariatti, M. A review on advanced carbon-based thermal interface materials for electronic devices. *Carbon* **2020**, *168*, 65–112. [CrossRef]
2. Sidhu, S.S.; Kumar, S.; Batish, A. Metal matrix composites for thermal management: A review. *Crit. Rev. Solid State Mater. Sci.* **2016**, *41*, 132–157. [CrossRef]
3. Xu, X.; Chen, J.; Zhou, J.; Li, B. Thermal Conductivity of Polymers and Their Nanocomposites. *Adv. Mater.* **2018**, *30*, 1705544. [CrossRef] [PubMed]
4. Shahil, K.M.; Balandin, A.A. Thermal properties of graphene and multilayer graphene: Applications in thermal interface materials. *Solid State Commun.* **2012**, *152*, 1331–1340. [CrossRef]
5. Hu, Y.; Chiang, S.W.; Chu, X.; Li, J.; Gan, L.; He, Y.; Li, B.; Kang, F.; Du, H. Vertically aligned carbon nanotubes grown on reduced graphene oxide as high-performance thermal interface materials. *J. Mater. Sci.* **2020**, *55*, 9414–9424. [CrossRef]
6. Chen, H.; Ginzburg, V.V.; Yang, J.; Yang, Y.; Liu, W.; Huang, Y.; Du, L.; Chen, B. Thermal conductivity of polymer-based composites: Fundamentals and applications. *Prog. Polym. Sci.* **2016**, *59*, 41–85. [CrossRef]
7. Hussain, A.R.J.; Alahyari, A.A.; Eastman, S.A.; Thibaud-Erkey, C.; Johnston, S.; Sobkowicz, M.J. Review of polymers for heat exchanger applications: Factors concerning thermal conductivity. *Appl. Therm. Eng.* **2017**, *113*, 1118–1127. [CrossRef]
8. Li, S.; Liu, B.; Jia, X.; Xu, M.; Zong, R.; Liu, G.; Huai, X. Optimization of thermal conductivity of alumina-filled composites by numerical simulations. *J. Therm. Sci.* **2023**, *32*, 1569–1582. [CrossRef]
9. Dirè, S.; Borovin, E.; Ribot, F. Architecture of Silsesquioxanes. In *Handbook of Sol-Gel Science and Technology*; Klein, L., Aparicio, M., Jitianu, A., Eds.; Springer International Publishing: Cham, Switzerland, 2016; pp. 1–34.
10. Loy, D.A. Sol–gel processing of hybrid organic–inorganic materials based on polysilsesquioxanes. In *Hybrid Materials. Synthesis, Characterization, and Applications*; Kickelbick, G., Ed.; Wiley: Weinheim, Germany, 2007; pp. 225–254.
11. Choi, S.S.; Lee, A.S.; Hwang, S.S.; Baek, K.Y. Structural control of fully condensed polysilsesquioxanes: Ladderlike vs cage structured polyphenylsilsesquioxanes. *Macromolecules* **2015**, *48*, 6063–6070. [CrossRef]

12. Kim, J.; Park, Y.; Kwon, M.S. Recent progress in ladder-like polysilsesquioxane: Synthesis and applications. *Mater. Chem. Front.* **2024**. [CrossRef]
13. Ren, Z.; Yan, S. Polysiloxanes for optoelectronic applications. *Prog. Mater. Sci.* **2016**, *83*, 383–416. [CrossRef]
14. Jo, Y.Y.; Lee, A.S.; Baek, K.Y.; Lee, H.; Hwang, S.S. Thermally reversible self-healing polysilsesquioxane structure-property relationships based on Diels-Alder chemistry. *Polymer* **2017**, *108*, 58–65. [CrossRef]
15. Kowalewska, A.; Nowacka, M.; Makowski, T.; Michalski, A. Thermal stability of self-assembled surfaces and micropatterns made of ladder polysilsesquioxanes. *Polymer* **2016**, *90*, 147–155. [CrossRef]
16. Hwang, S.O.; Lee, A.S.; Lee, J.Y.; Park, S.H.; Jung, K.I.; Jung, H.W.; Lee, J.H. Mechanical properties of ladder-like polysilsesquioxane-based hard coating films containing different organic functional groups. *Prog. Org. Coat.* **2018**, *121*, 105–111. [CrossRef]
17. Oh, H.; Jo, E.; Jang, H.W.; Jung, H.; Park, S.H.; Kim, A.Y.; Jung, J.H.; Youk, J.H.; Lee, M. Hard coating films of fluorine-containing ladder-like structured polysilsesquioxane as negative triboelectric materials for high-performance triboelectric generators. *Extrem. Mech. Lett.* **2022**, *50*, 101533. [CrossRef]
18. Wang, Q.; Zhang, H.; Cui, Z.; Zhou, Q.; Shangguan, X.; Tian, S.; Zhou, X.; Cui, G. Siloxane-based polymer electrolytes for solid-state lithium batteries. *Energy Storage Mater.* **2019**, *23*, 466–490. [CrossRef]
19. Kim, Y.H.; Choi, G.M.; Bae, J.G.; Kim, Y.H.; Bae, B.S. High-performance and simply-synthesized ladder-like structured methacrylate siloxane hybrid material for flexible hard coating. *Polymers* **2018**, *10*, 449. [CrossRef] [PubMed]
20. Lee, A.S.; Choi, S.S.; Lee, H.S.; Jeon, H.Y.; Baek, K.Y.; Hwang, S.S. Thermal, Optical, and Film Properties of a Ladder-like Polysilsesquioxane as Flexible Electronic Device Substrates. *MRS Online Proc. Libr. (OPL)* **2012**, *1436*, mrss12-1436. [CrossRef]
21. Shin, Y.K.; Lee, W.S.; Yoo, M.J.; Kim, E.S. Effect of BN filler on thermal properties of HDPE matrix composites. *Ceram. Int.* **2013**, *39*, S569–S573. [CrossRef]
22. Liu, J.; Fang, Z.; Bao, C. Studies on 8.4 W/m· K thermally conductive silicone rubber with high compressibility, high electrical insulation, high thermal reliability, and low cost. *Compos. A Appl. Sci. Manuf.* **2024**, *180*, 108100. [CrossRef]
23. Mirizzi, L.; D'Arienzo, M.; Nisticò, R.; Fredi, G.; Diré, S.; Callone, E.; Dorigato, A.; Giannini, L.; Guerra, S.; Mostoni, S.; et al. Al_2O_3 decorated with polyhedral silsesquioxane units: An unconventional filler system for upgrading thermal conductivity and mechanical properties of rubber composites. *Compos. Sci. Technol.* **2023**, *236*, 109977. [CrossRef]
24. Kochetov, R.; Korobko, A.V.; Andritsch, T.; Morshuis, P.H.F.; Picken, S.J.; Smit, J.J. Modelling of the thermal conductivity in polymer nanocomposites and the impact of the interface between filler and matrix. *J. Phys. D Appl. Phys.* **2011**, *44*, 395401. [CrossRef]
25. Khan, W.S.; Asmatulu, R.; Ahmed, I.; Ravigururajan, T.S. Thermal conductivities of electrospun PAN and PVP nanocomposite fibers incorporated with MWCNTs and NiZn ferrite nanoparticles. *Int. J. Therm. Sci.* **2013**, *71*, 74–79. [CrossRef]
26. Ouyang, Y.; Ding, F.; Bai, L.; Li, X.; Hou, G.; Fan, J.; Yuan, F. Design of network Al_2O_3 spheres for significantly enhanced thermal conductivity of polymer composites. *Compos. A Appl. Sci. Manuf.* **2020**, *128*, 105673. [CrossRef]
27. Mingarelli, P.; Romeo, C.; Callone, E.; Fredi, G.; Dorigato, A.; D'Arienzo, M.; Parrino, F.; Dirè, S. Ladder-like Poly (methacryloxypropyl) silsesquioxane-Al_2O_3-polybutadiene Flexible Nanocomposites with High Thermal Conductivity. *Gels* **2023**, *9*, 810. [CrossRef] [PubMed]
28. Ahn, Y.; Kim, S.; Kim, M.S.; Youk, J.H.; Kim, B.G. Ladder-Structured Polysilsesquioxane/Al_2O_3 Nanocomposites for Transparent Wear-Resistant Windows. *Fibers Polym.* **2018**, *19*, 1295–1302. [CrossRef]
29. Bounphanh, T.; Junchun, Y.; Ove, A. Effects of cross-links, pressure and temperature on the thermal properties and glass transition behaviour of polybutadiene. *Phys. Chem. Chem. Phys.* **2011**, *13*, 15047–15054.
30. Li, J.; Zhang, X.; Yuen, M.M.-F.; Liu, L.; Ku, C.S.; Zhang, K. Enhancing the Thermal Conductivity of Silicone Composites by Increasing Crosslink Degree. In Proceedings of the 15th International Conference on Electronic Packing Technology, Chengdu, China, 12–15 August 2014.
31. Ribas-Massonis, A.; Cicujano, M.; Duran, J.; Besalú, E.; Poater, A. Free-radical photopolymerization for curing products for refinish coatings market. *Polymers* **2022**, *14*, 2856. [CrossRef]
32. Corrigan, N.; Jung, K.; Moad, G.; Hawker, C.J.; Matyjaszewski, K.; Boyer, C. Reversible-deactivation radical polymerization (Controlled/living radical polymerization): From discovery to materials design and applications. *Prog. Polym. Sci.* **2020**, *111*, 101311. [CrossRef]
33. Shim, G.S.; Kim, J.S.; Kim, H.J. Behavior and adhesion performance of acrylic PSAs using Semi-IPN structure and UV/UV stepwise curing. *J. Ind. Eng. Chem.* **2020**, *89*, 139–146. [CrossRef]
34. Ligon, S.C.; Husár, B.; Wutzel, H.; Holman, R.; Liska, R. Strategies to reduce oxygen inhibition in photoinduced polymerization. *Chem. Rev.* **2014**, *114*, 557–589. [CrossRef] [PubMed]
35. Dumur, F. The future of visible light photoinitiators of polymerization for photocrosslinking applications. *Eur. Polym. J.* **2023**, *187*, 111883. [CrossRef]
36. Kraśkiewicz, A.; Kowalczyk, A.; Kowalczyk, K.; Markowska-Szczupak, A.; Idzik, T.J.; Sośnicki, J.G. Anticorrosive and antimicrobial efficiency of photopolymerizable phosphorus (meth) acrylate oligomers-based coating materials. *Prog. Org. Coat.* **2024**, *187*, 108141. [CrossRef]
37. Sivanesan, D.; Seo, B.; Lim, C.S.; Kim, H.; Kim, H.G. Intramolecular hydrogen-bond-based latent initiator for olefin metathesis polymerization. *Organometallics* **2021**, *40*, 314–323. [CrossRef]

38. Żak, P.; Pietraszuk, C. Application of olefin metathesis in the synthesis of functionalized polyhedral oligomeric silsesquioxanes (POSS) and POSS-containing polymeric materials. *Beilstein J. Org. Chem.* **2019**, *15*, 310–332. [CrossRef] [PubMed]
39. Jiang, B.; Shi, X.; Zhang, T.; Huang, Y. Recent advances in UV/thermal curing silicone polymers. *Chem. Eng. J.* **2022**, *435*, 134843. [CrossRef]
40. Dirè, S.; Callone, E.; Ceccato, R.; Parrino, F.; Di Credico, B.; Mostoni, S.; Scotti, R.; D'Arienzo, M. Structural effects of TiO_2 nanoparticles in photocurable ladder-like polysilsesquioxane nanocomposites. *J. Sol-Gel Sci. Technol.* **2023**, 1–13. [CrossRef]
41. D'Arienzo, M.; Diré, S.; Masneri, V.; Rovera, D.; Di Credico, B.; Callone, E.; Mascotto, S.; Pegoretti, A.; Ziarelli, F.; Scotti, R. Tailoring the dielectric and mechanical properties of polybutadiene nanocomposites by using designed ladder-like polysilsesquioxanes. *ACS Appl. Nano Mater.* **2018**, *1*, 3817–3828. [CrossRef]
42. Soo Lee, A.S.; Lee, J.H.; Lee, J.-C.; Hong, S.M.; Hwang, S.S.; Koo, C.M. Novel polysilsesquioxane hybrid polymer electrolytes for lithium ion batteries. *J. Mater. Chem. A* **2014**, *2*, 1277–1283. [CrossRef]
43. Borovin, E.; Callone, E.; Papendorf, B.; Guella, G.; Diré, S. Influence of sol–gel conditions on the growth of thiolfunctionalized silsesquioxanes prepared by in situ water production. *J. Nanosci. Nanotechnol.* **2016**, *16*, 3030–3038. [CrossRef]
44. Zamperlin, N.; Bottacini, A.; Callone, E.; Pegoretti, A.; Fontana, M. Barium titanate functionalization with organosilanes: Effect on particle compatibility and permittivity in nanocomposites. *Molecules* **2022**, *27*, 6499. [CrossRef]
45. Zhang, Z.M.; Zhang, Z.M.; Luby. *Nano/Microscale Heat Transfer*, 2nd ed.; Springer Nature: Cham, Switzerland, 2020.